Ultrathin Trimetal−Organic Framework Nanosheet Electrocatalysts for the Highly Efficient Oxygen Evolution Reaction

Songyang Niu, Chenhui Li, Jia Huo,* Wanrong Dong,* Samir El Hankari,* Yu Liang, and Qiling Li

ACCESS | Metrics & More | Article Recommendations | SI Supporting Information

ABSTRACT: Synthesis of ultrathin metal−organic framework (MOF) nanosheets for highly efficient oxygen evolution reaction (OER) is prevalent, but still many challenges remain. Herein, a facile and efficient three-layer method is reported for the synthesis of NiCoFe-based trimetallic MOF nanosheets, which can be directly used for the oxygen evolution reaction in alkaline conditions. The physical characterization and morphology of trimetallic MOF nanosheets were characterized by powder X-ray diffraction (PXRD), X-ray photoelectron spectroscopy (XPS), scanning electron microscopy (SEM), and transmission electron microscopy (TEM). By optimizing the molar ratio of Ni/Co/Fe atoms, a series of MOFs with different metal proportions were synthesized. Among them, the as-prepared $(Ni_3Co_1)_3Fe_1$-MOF nanosheets can deliver a current density of 10 mA cm^{-2} at a low overpotential of 245 mV with a small Tafel slope of 50.9 mV dec^{-1} in an alkaline electrolyte and exhibit excellent stability. More importantly, through the characterization of the intermediates in the OER process, the possible source of the catalytic active species is the electrochemically transformed metal hydroxides and oxyhydroxides.
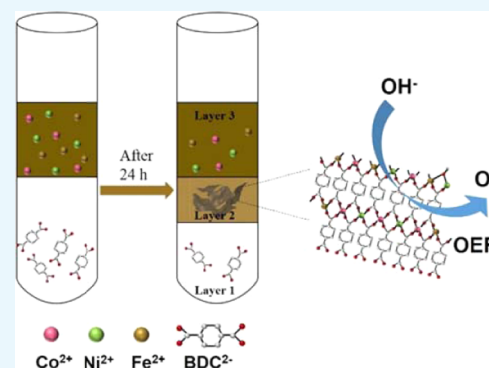
INTRODUCTION

Under the pressure of global warming and huge consumption of fossil energy, it is imperative to develop eco-friendly and efficient energy resources (e.g., fuel cells,[1,2] batteries,[3,4] electrocatalytic water splitting[5,6]). Oxygen evolution reaction (OER) plays an important role in metal−air batteries and electrocatalytic water splitting. However, the sluggish kinetics of OER, which involves the multistep proton-coupled transfer of four electrons, needs to be resolved urgently, where the design of highly efficient catalysts is one of the crucial issues for OER. As is well known, nanosized materials possess large specific surface area, abundant exposed active sites, and rapid electron transfer rates. In view of this finding, reducing the size of electrocatalysts is an effective strategy to improve the electrocatalytic activity of the OER. Since graphene was discovered through the exfoliation of graphite in 2004, two-dimensional (2D) nanomaterials, such as layered metal oxides,[7,8] graphitic carbon nitride,[9] transition-metal dichalcogenides,[10] lactic dehydrogenases (LDH),[11] and metal−organic frameworks (MOFs),[12,13] have attracted much more attention because of their unique physical and chemical properties. These materials have been widely applied in many fields, such as gas separation, energy storage, and electronic and optoelectronic devices.

Recently, MOFs have emerged as novel OER catalysts because of their tunable porosity, high specific surface area, and diversity in the functional species of metal centers and organic linkers. Turning three-dimensional (3D) bulk MOFs into 2D MOFs have the following advantages: (i) ultrathin nanostructures expose more active sites; (ii) increased specific surface area allows the active sites to be in full contact with the reactants; and (iii) these ultrathin nanostructures easily form more defects to produce more coordination-unsaturated metal sites, which can reduce the reactive energy barrier by optimizing the charge structure. Tang et al.[14] demonstrated the OER performance of ultrathin NiCo-MOF nanosheets, which presented a low overpotential of 250 mV at 10 mA cm^{-2} in alkaline conditions, far below that of bulk NiCo-MOFs (317 mV). Pang et al.[15] reported a one-pot hydrothermal method to synthesize ultrathin 2D Co-MOF nanosheets, and the obtained 2D Co-MOF nanosheets have higher OER activity than that of bulk MOFs. These indicate that the 2D MOF nanosheets will get increasing attention in the area of electrocatalytic water splitting, which relies on their distinctive physical and chemical properties. Recent reports have demonstrated that Ni-, Fe-, and Co-based MOFs have excellent catalytic performance in the field of electrocatalytic water splitting.[16−18] Furthermore, the doping of nickel−cobalt−iron ternary metal results in a change in the electronic structure,[19−21] thereby improving the conductivity of the MOFs. Therefore, by embedding the

nickel—cobalt—iron ternary metal into large-size MOF nano-sheets, the catalytic performance of the catalysts is greatly improved.

Here, we prepared ultrathin trimetal—organic framework nanosheets by a three-layer method with Ni^{2+}, Co^{2+}, and Fe^{2+} ions and benzene dicarboxylate (BDC) ligands in separate phases, favoring the formation of ultrathin MOF nanosheets (MOFNSs) between the interface layer. Impressively, the as-synthesized $(Ni_3Co_1)_3Fe_1$-MOFNSs demonstrated excellent electrocatalytic OER activity in alkaline conditions with a low overpotential of 245 mV at 10 mA cm^{-2}, a small Tafel slope of 50.9 mV dec^{-1}, and outstanding electrochemical stability for at least 30 000 s. Meanwhile, the possible active species during the OER process are revealed to be the electrochemically transformed metal hydroxides and oxyhydroxides based on the high-resolution XPS spectra, XRD, and the ex situ Raman spectra results.

■ RESULTS AND DISCUSSION

The ultrathin NiCoFe-MOF nanosheets were synthesized by a three-layer method based on the diffusion-mediated regulation of the MOF growth. The corresponding synthetic process is illustrated in Scheme 1. Typically, mixtures of *N,N*-

Scheme 1. Schematic Illustration of the Synthesis of $(Ni_3Co_1)_3Fe_1$-MOFNSs
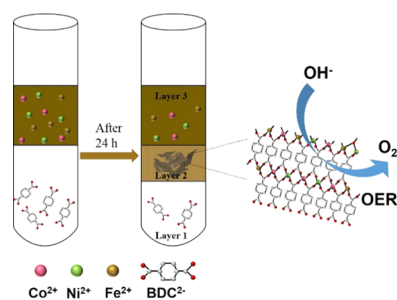
dimethylformamine (DMF) and acetonitrile (CH$_3$CN) with different volume ratios (V_{DMF}/V_{CH_3CN}) were prepared for each layer with 2:1 for layer 1, 1:1 for layer 2, and 1:2 for layer 3. First, 10 mg of H$_2$BDC was dissolved in layer 1 at the bottom of a glass tube. Then, the mixture of DMF and CH$_3$CN of layer 2 was carefully added on the top of layer 1. Finally, certain amounts of Co(CH$_3$COO)$_2$·4H$_2$O, Ni(CH$_3$COO)$_2$·4H$_2$O, and Fe(CH$_3$COO)$_2$ were dissolved in the solvents of layer 3. After keeping for 24 h, the MOF solids were accumulated in layer 2, and some of them were deposited at the bottom of the glass tube under gravity. The atomic ratio of the Ni/Co/Fe could be easily controlled by adjusting the amount of metal salts. The detailed synthetic procedures are described in the Experimental Section.

The morphology of the as-synthesized sample could be observed by scanning electron microscopy (SEM; Figure 1a) and transmission electron microscopy (TEM; Figure 1b), where the morphology of ultrathin nanosheets could be revealed. The thickness of $(Ni_3Co_1)_1Fe_1$-MOFNSs was determined to be 8.15 nm via atomic force microscopy (AFM; Figure 1c), and their excellent dispersion in aqueous solution could be observed by the Tyndall effect under laser irradiation (inset of Figure 1c). The $(Ni_3Co_1)_1Fe_1$-MOFNSs and bulk $(Ni_3Co_1)_1Fe_1$-MOFs have similar XRD peaks, and the powder X-ray diffraction (PXRD) patterns are in agreement
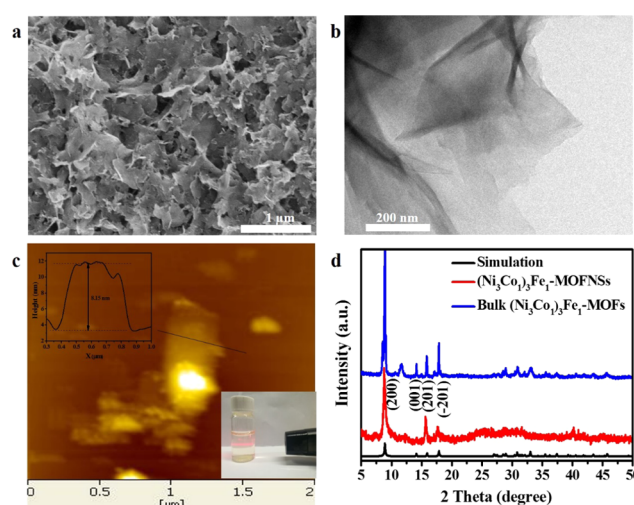
Figure 1. (a) SEM image of $(Ni_3Co_1)_3Fe_1$-MOFNSs. (b) TEM image of $(Ni_3Co_1)_3Fe_1$-MOFNSs. (c) AFM image of $(Ni_3Co_1)_3Fe_1$-MOFNSs. The Tyndall effect under laser irradiation corresponds to the AFM image in (c). (d) PXRD pattern of $(Ni_3Co_1)_3Fe_1$-MOFNSs and the bulk $(Ni_3Co_1)_3Fe_1$-MOFs.

with the previously reported 2D Ni-based MOFs[22] (Figure 1d), which suggest the successful synthesis of ultrathin MOF nanosheets. In this crystal structure, the Ni, Co, and Fe atoms are octahedrally coordinated by six O atoms to form 2D mixed-metal oxide layers, which are pillared with benzene dicarboxylate (BDC) ligands. The powder X-ray diffraction (PXRD) patterns of different metal ratios of NiCoFe-MOFNSs are also similar (Figure S1). The Fourier transformation infrared spectrometry (FT-IR) spectra reveal that the as-synthesized samples and bulk MOFs have the same peaks, indicating they have similar functional groups (Figure S2). The specific surface area and pore size distribution of $(Ni_3Co_1)_1Fe_1$-MOFNSs were 62.6 cm^2 g^{-1} and 4.16 nm, respectively, which were analyzed from its N$_2$ adsorption/desorption isotherm (Figure S3a,b).

The electrocatalytic OER activities of these MOFs were investigated by linear sweep voltammetry (LSV) in 1.0 M KOH on a glassy carbon electrode (GCE) at room temperature using graphite rod as the counter electrode. The $(Ni_3Co_1)_1Fe_1$-MOFNSs exhibit higher electrocatalytic OER activity than the bulk $(Ni_3Co_1)_1Fe_1$-MOFs and commercial RuO$_2$. The performance of $(Ni_3Co_1)_1Fe_1$-MOFNSs requires an overpotential of 245 mV at a current density of 10 mA cm^{-2}, much smaller than that of bulk $(Ni_3Co_1)_1Fe_1$-MOFs (294 mV), commercial RuO$_2$ (306 mV), and other different metal ratio MOFNS electrocatalysts (Figure 2a). The $(Ni_3Co_1)_1Fe_1$-MOFNSs display highly enhanced OER activity when compared to the known MOF-based OER electrocatalysts, which make use of nonprecious metals in alkaline media (Table S1). Then, the corresponding Tafel slope for the $(Ni_3Co_1)_1Fe_1$-MOFNSs (50.9 mV dec^{-1}) is also lower than that of the bulk $(Ni_3Co_1)_1Fe_1$-MOFs (76.8 mV dec^{-1}) and other different metal ratio electrocatalysts (Figure 2b). The double-layer capacitances (C_{dl}) of MOFNs were evaluated by cyclic voltammetry (CV). The electrochemically active surface areas (ESCA) of MOFNSs were compared as the C_{dl} is linearly proportional to the ESCA. To understand the OER activity of MOF nanosheets, we measured the double-layer capacitances (C_{dl}) of $(Ni_3Co_1)_3Fe_1$-MOFNSs and bulk $(Ni_3Co_1)_3Fe_1$-MOFs
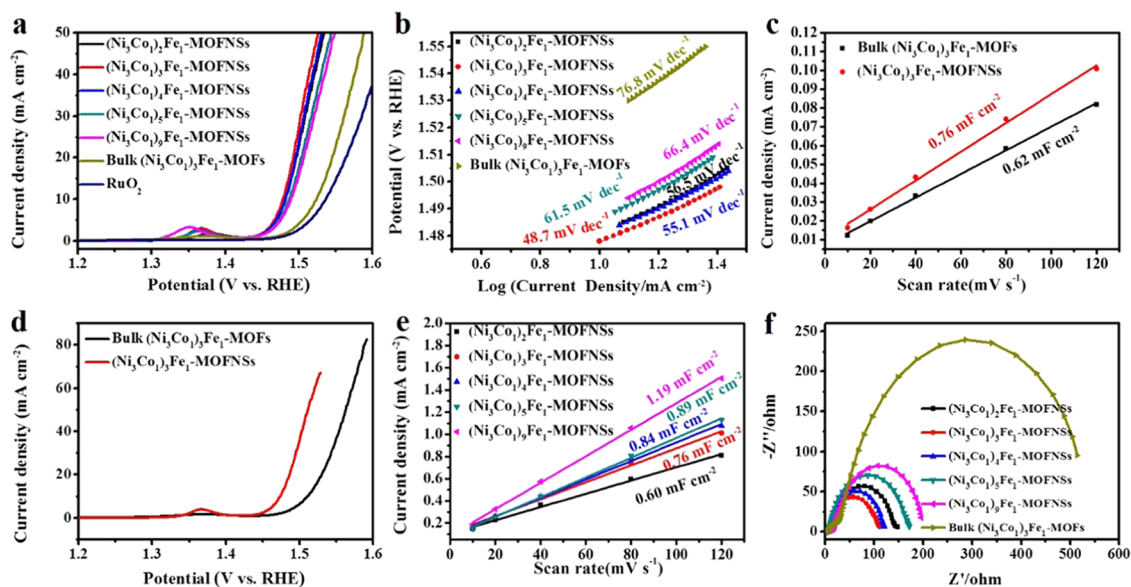
Figure 2. OER performance of different metal proportions in MOFNSs. (a) LSV curves for the OER at a scan rate of 5 mV s^{-1}. (b) The corresponding Tafel plots. (c) Double-layer capacitances (C_{dl}) of the $(Ni_3Co_1)_3Fe_1$-MOFNSs and the bulk $(Ni_3Co_1)_3Fe_1$-MOFs. (d) LSV curves normalized by ECSA of the $(Ni_3Co_1)_3Fe_1$-MOFNSs and the bulk $(Ni_3Co_1)_3Fe_1$-MOFs. (e) Double-layer capacitances (C_{dl}) of different metal proportions in MOFNSs. (f) Nyquist plots at an overpotential of 220 mV.

by cyclic voltammetry (CV) in a non-Faradic region (Figure S4a,b). $(Ni_3Co_1)_3Fe_1$-MOFNSs exhibited higher values of C_{dl} (0.76 mF cm^{-2}) than bulk $(Ni_3Co_1)_3Fe_1$-MOFs (0.62 mF cm^{-2}) (Figure 2c), suggesting that $(Ni_3Co_1)_3Fe_1$-MOFNSs could expose more active sites. To reveal the intrinsic activities of MOFs, the LSV curves of $(Ni_3Co_1)_3Fe_1$-MOFNSs and bulk $(Ni_3Co_1)_3Fe_1$-MOFs were normalized by ECSA (Figure 2d). The $(Ni_3Co_1)_3Fe_1$-MOFNSs showed better OER activity compared with the bulk $(Ni_3Co_1)_3Fe_1$-MOFs, which indicated that the intrinsic activity of the $(Ni_3Co_1)_3Fe_1$-MOFNSs was improved. The double-layer capacitances (C_{dl}) of different metal ratio NiCoFe-MOFNSs were also determined by cyclic voltammetry (CV) (Figure S5a–d). The slope is linear with the iron content, indicating that iron could influence the electrochemical surface area (ECSA) (Figure 2e). To further understand the OER reaction kinetics, electrochemical impedance spectroscopy (EIS) was conducted at an applied potential of 1.45 V (versus reversible hydrogen electrode (RHE)). The electrochemical impedance spectroscopy (EIS) was used to gain insight into the charge-transfer process between the catalyst and the electrolyte, which could further evaluate the electrode reaction kinetic of OER (Figures 2f and S6a,b). The $(Ni_3Co_1)_1Fe_1$-MOFNSs exhibited a smaller charge-transfer resistance (105 Ω) than the bulk $(Ni_3Co_1)_1Fe_1$-MOFs (536 Ω) and other different metal ratio electrocatalysts, confirming that the $(Ni_3Co_1)_1Fe_1$-MOFNSs had a faster charge transfer than the bulk $(Ni_3Co_1)_1Fe_1$-MOFs and other different metal ratio electrocatalysts in the OER process. Furthermore, there was a little change in the OER performance after 1000, 2000, and 3000 CV cycles, respectively (Figure 3a). The $(Ni_3Co_1)_1Fe_1$-MOFNSs also exhibited excellent long-time stability (Figure 3b).

For the purpose of investigating the OER active species of $(Ni_3Co_1)_1Fe_1$-MOFNSs in the electrocatalytic OER process, we monitored the change in the structure and electronic state of electrocatalysts through the observation of the intermediates after different CV cycles. It was obvious that the PXRD notably changed after 10 CV cycles compared to the original MOFNS
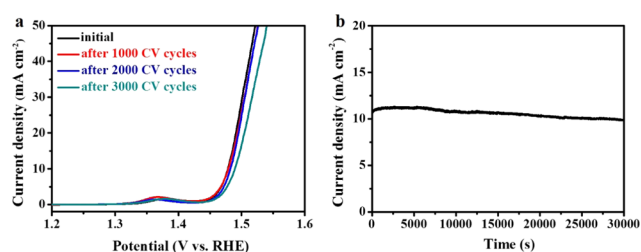

Figure 3. (a) Polarization curves of the $(Ni_3Co_1)_3Fe_1$-MOFNSs before and after 1000, 2000, and 3000 CV cycles, respectively. (b) I−t curve at an overpotential of 275 mV versus RHE.

structure. With the disappearance of original peaks, several new peaks appeared, which could be ascribed to $Co(OH)_2$ (JCPDS No. 45-0031), FeOOH (JCPDS No. 46-1436), and NiOOH (JCPDS No. 06-0075)[23−25] (Figure 4a). Raman vibrational peaks for $(Ni_3Co_1)_3Fe_1$-MOFNSs were observed at 1609, 1435, 1135, 862, and 633 cm^{-1}, respectively. However, after 10

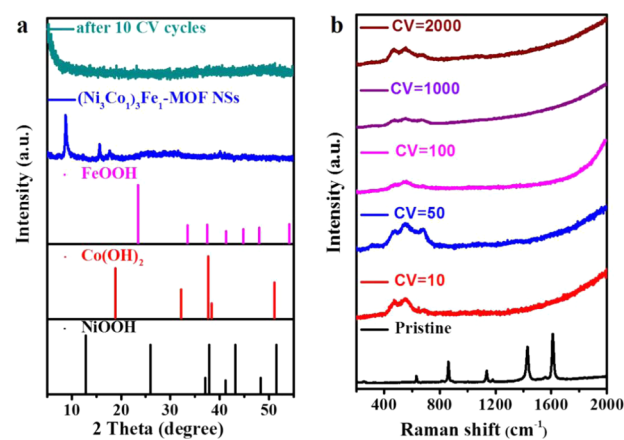**Figure 4.** (a) XRD patterns and (b) Raman spectra of $(Ni_3Co_1)_3Fe_1$-MOFNSs after different CV tests.

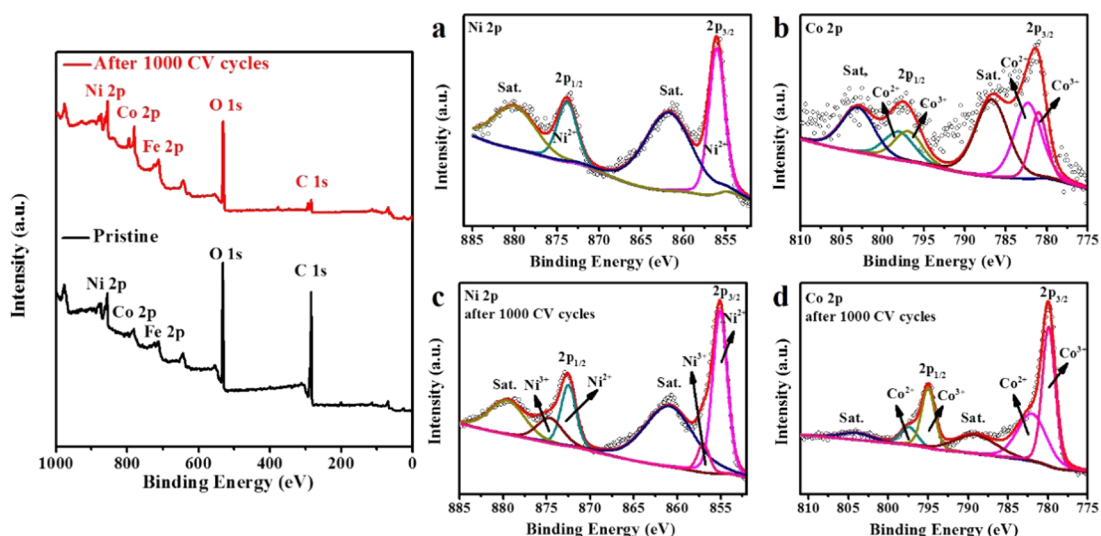**Figure 5.** Survey spectrum of the $(Ni_3Co_1)_3Fe_1$-MOFNSs before and after 1000 CV cycles. (a) Ni 2p XPS of the $(Ni_3Co_1)_3Fe_1$-MOFNSs. (b) Co 2p XPS of the $(Ni_3Co_1)_3Fe_1$-MOFNSs. (c) Ni 2p XPS of the $(Ni_3Co_1)_3Fe_1$-MOFNSs after 1000 CV cycles. (d) Co 2p XPS of the $(Ni_3Co_1)_3Fe_1$-MOFNSs after 1000 CV cycles.

CV cycles, original peaks disappeared and three new peaks were observed 467, 550, and 650 cm^{-1}, respectively, originating from the A_{1g} stretching modes of Ni−OH in the $Ni(OH)_2$, e_g bending vibration of Ni−O in the NiOOH, and the bending vibration of Co−O[26,27] (Figure 4b). The FT-IR analysis also confirms the structural evolution with the absorption peaks at 3606 cm^{-1} completely disappearing after 10 cycles, while a new absorption peak appears at 550 cm^{-1} derived from the Ni−O vibration (Figure S7).

The surface chemical valence states of electrocatalysts before and after OER were studied by XPS analysis (Figure 5). The high-resolution XPS spectra of Co 2p after 1000 cycles (Figure 5b,d) clearly reflect that the peaks are shifted to lower binding energy (Co $2p_{3/2}$ at 782 and 779.9 eV, Co $2p_{1/2}$ at 797.4 and 779.9 eV) compared to those of the pristine MOFNSs (Co $2p_{3/2}$ at 782.3 and 781 eV, Co $2p_{1/2}$ at 796.9 and 786.7 eV). The negative shift of binding energy for Co $2p_{3/2}$ and $2p_{1/2}$ can be ascribed to the destruction of the metal−organic ligand, which results in a change in the local electronic structure and the possible structural evolution from MOFNSs to $Co(OH)_2$ and CoOOH.[28,29] Similarly, the Ni 2p peaks reflected the new peaks of Ni $2p_{3/2}$ and Ni $2p_{1/2}$ at 857.0 and 874.6 eV,[30,31] respectively, corresponding to Ni^{3+}, confirming the formation of NiOOH during the electrocatalytic process (Figure 5a,c). In the Fe 2p spectrum, the binding energy peak at 712.6 eV is attributed to Fe $2p_{3/2}$, which means the existence of Fe^{3+}. After 1000 cycles, the binding energy of Fe $2p_{2/3}$ shifts to 711.0 eV due to the structural evolution[32] (Figure S8a,c). The O 1s XPS spectrum of the pristine $(Ni_3Co_1)_1Fe_1$-MOFNSs showed that the peak at 531.5, 532.5, and 533.5 eV were regarded as the M−O−R, O = C−O, and O−H bonds, respectively (Figure S8b). After 1000 CV cycles, change in the electronic structure of O 1s was also evidenced by the binding energy shift, where the peaks of O 1 s shifted to a lower binding energy[33] (531.6 eV from −OH, 530.7 eV from M−OH and 529.4 eV from M−O group), further indicating the possible formation of hydroxide and oxyhydroxide during the OER process (Figure S8d).

CONCLUSIONS

In summary, we demonstrated a three-layer method to synthesize ultrathin trimetal−organic framework nanosheets, which acted as high-performance catalysts in the OER. By adjusting the ratio of Ni/Co/Fe, the $(Ni_3Co_1)_3Fe_1$-MOFNSs exhibited the optimal OER activity with an overpotential of 245 mV at 10 mA cm^{-2} in alkaline conditions and a small Tafel slope of 50.9 mV dec^{-1}. More importantly, through the study of intermediates during the OER process, it was found that the electrochemically transformed metal hydroxide and oxyhydroxide evolved from the pristine MOFNSs could be the active species. This work provides a new method for the synthesis of MOF nanosheets electrocatalysts and also stimulates the study of active species in the electrocatalytic process of pristine MOFs.

EXPERIMENTAL SECTION

Chemicals. Nickel(II) acetate $(Ni(CH_3COO)_2 \cdot 4H_2O)$, cobalt(II) acetate tetrahydrate $(Co(CH_3COO)_2 \cdot 4H_2O)$, and ferrous acetate $(Fe(CH_3COO)_2)$ were purchased from Sinopharm Chemical Reagent Co. Ltd. (Shanghai, China). 1,4-Benzene dicarboxylic acid (1,4-H_2BDC) was purchased from Adamas. *N,N*-Dimethylformamide (DMF) and acetonitrile (CH_3CN) were purchased form Energy Chemical. Ultrapure water (18.25 MΩ) used in the experiments was supplied by a Millipore System (Millipore Q).

Synthesis of Materials. *Synthesis of $(Ni_3Co_1)_3Fe_1$-MOFNSs.* The $(Ni_3Co_1)_3Fe_1$-MOFNSs were synthesized in a glass tube by a diffusion-mediated method. Typically, 0.06 mmol of 1,4-H_2BDC was dissolved in a mixture of 2 mL of DMF and 1 mL of CH_3CN and then poured into the bottom of the glass tube. On top of this solution, a mixture of 1 mL of DMF and 1 mL of CH_3CN was carefully added as the spacer layer. The metal precursors 0.03375 mmol $Ni(CH_3COO)_2 \cdot 4H_2O$, 0.01125 mmol $Co(CH_3COO)_2 \cdot 4H_2O$, and 0.015 mmol $(Fe(CH_3COO)_2)$ were dissolved in a mixture of 1 mL of DMF and 2 mL of CH_3CN. Finally, the solution was also carefully added to the glass tube as the top layer. The synthesis proceeded at room temperature for 24 h under static conditions. The collected precipitate was centrifuged and

washed with DMF and ethanol several times and dried at 60 °C for 12 h.

Synthesis of Bulk (Ni₃Co₁)₃Fe₁-MOFs. Typically, 0.6 mmol 1,4-H_2BDC and 0.3375 mmol $Ni(CH_3COO)_2 \cdot 4H_2O$, 0.1125 mmol $Co(CH_3COO)_2 \cdot 4H_2O$, and 0.15 mmol ($Fe(CH_3COO)_2$), and 15 mL of N,N-dimethylformamide (DMF) were mixed in a 25 mL round-bottom flask and refluxed at 100 °C during 24 h. The resulting powder was collected by centrifugation at 8000 rpm, and the solid was consecutively washed three times with DMF (20 mL each step), followed by washing three times with $CHCl_3$ (20 mL each step) to efficiently remove the remaining linker molecules, which might have remained occluded in the MOF pores after the synthesis.

Characterization. The morphology of all electrocatalysts was investigated by scanning electron microscopy (SEM, Hitachi, S-4800) and transmission electron microscopy (JEM3010). The size and thickness of the electrocatalysts were determined by atomic force microscopy (AFM, Brucker Bioscope system). The crystal structures of the samples were characterized using powder X-ray diffraction (XRD, Bruker D8 Advance diffractometer, Cu Kα1). Nitrogen adsorption/desorption isotherms were measured by JW-BK200C (JWGB SCI.&.TECH.) at the desired temperature, and the samples were dried for 12 h at 423 K under vacuum before the measurement. The Raman spectra were collected on a Raman spectrometer (Invia-reflex) using a 633 nm laser. The X-ray photoelectron spectroscopy (XPS) analysis was performed on an ESCALAB 250Xi X-ray photoelectron spectrometer using Mg as the excitation source. The infared spectrum tests were performed at the Fourier transformation infrared spectrometer (FT-IR, Infinity-1).

Electrochemical Measurements. All of the electrochemical measurements were performed with a CHI 760D electrochemical workstation. OER was performed in a three-electrode configuration. For electrochemical measurement of OER, the catalyst dropped on a glassy carbon electrode was used as the working electrode, saturated calomel electrode (SCE) was used as the reference electrode in 1 M KOH electrolyte, and platinum gauze was used as the counter electrode. The scan rate for linear sweep voltammetry (LSV) was kept at 5 mV s⁻¹ to minimize the capacitive current. In addition, the LSV polarization curves for the OER was measured after saturating the solution with O_2. Before recording the catalytic activity, the catalysts were activated by a chronopotentiometry scan with a constant current density until reaching a stable state. All of the polarization curves in this work were corrected by eliminating the IR drop with respect to the ohmic resistance of the solution. Calibration of SCE reference electrodes was done by measuring the reversible hydrogen electrode (RHE) potential using a Pt electrode under a H_2 atmosphere.[34] All potentials were normalized to a reversible hydrogen electrode (RHE) according to the equation[35] $E(\text{RHE}) = E(\text{SCE}) + 0.242\text{V} + 0.0591\text{pH}$. Span life measurements were performed to evaluate the long-term stability. The impedance spectra of OER was measured in the three-electrode system under 1.45 V versus RHE over the frequency range from 1 MHz to 0.1 Hz in 1.0 M KOH using Autolab.

■ AUTHOR INFORMATION

Corresponding Authors

Jia Huo — State Key Laboratory of Chem/Bio-Sensing and Chemometrics, Provincial Hunan Key Laboratory for Graphene Materials and Devices, College of Chemistry and Chemical Engineering, Hunan University, Changsha, Hunan 410082, China; Hunan Provincial Key Laboratory of Advanced Materials for New Energy Storage and Conversion, Hunan University of Science and Technology, Xiangtan 411201, China; ⓞ orcid.org/0000-0002-6187-3847; Email: jiahuo@hnu.edu.cn

Wanrong Dong — State Key Laboratory of Chem/Bio-Sensing and Chemometrics, Provincial Hunan Key Laboratory for Graphene Materials and Devices, College of Chemistry and Chemical Engineering, Hunan University, Changsha, Hunan 410082, China; ⓞ orcid.org/0000-0002-6541-2853; Email: wanrongdong@hnu.edu.cn

Samir El Hankari — State Key Laboratory of Chem/Bio-Sensing and Chemometrics, Provincial Hunan Key Laboratory for Graphene Materials and Devices, College of Chemistry and Chemical Engineering, Hunan University, Changsha, Hunan 410082, China; Chemical and Biochemical Science Department, Mohammed VI Polytechnic University, Ben Guerir 43150, Morocco; Email: elhankarisamir@gmail.com

Authors

Songyang Niu — State Key Laboratory of Chem/Bio-Sensing and Chemometrics, Provincial Hunan Key Laboratory for Graphene Materials and Devices, College of Chemistry and Chemical Engineering, Hunan University, Changsha, Hunan 410082, China

Chenhui Li — State Key Laboratory of Chem/Bio-Sensing and Chemometrics, Provincial Hunan Key Laboratory for Graphene Materials and Devices, College of Chemistry and Chemical Engineering, Hunan University, Changsha, Hunan 410082, China

Yu Liang — State Key Laboratory of Chem/Bio-Sensing and Chemometrics, Provincial Hunan Key Laboratory for Graphene Materials and Devices, College of Chemistry and Chemical Engineering, Hunan University, Changsha, Hunan 410082, China

Qiling Li — State Key Laboratory of Chem/Bio-Sensing and Chemometrics, Provincial Hunan Key Laboratory for Graphene Materials and Devices, College of Chemistry and Chemical Engineering, Hunan University, Changsha, Hunan 410082, China

Complete contact information is available at:
https://pubs.acs.org/10.1021/acsomega.0c01853

Notes

The authors declare no competing financial interest.

■ REFERENCES

(1) Ren, Y.; Chia, G. H.; Gao, Z. Metal-organic frameworks in fuel cell technologies. *Nano Today* **2013**, *8*, 577−597.

(2) Zhang, X.; Chen, A.; Zhong, M.; Zhang, Z.; Zhang, X.; Zhou, Z.; Bu, X.-H. Metal-Organic Frameworks (MOFs) and MOF-Derived Materials for Energy Storage and Conversion. *Electrochem. Energy Rev.* **2019**, *2*, 29−104.

(3) Fang, G.; Zhou, J.; Liang, C.; Pan, A.; Zhang, C.; Tang, Y.; Tan, X.; Liu, J.; Liang, S. MOFs nanosheets derived porous metal oxide-coated three-dimensional substrates for lithium-ion battery applications. *Nano Energy* **2016**, *26*, 57−65.

(4) Bai, Z.; Zhang, Y.; Zhang, Y.; Guo, C.; Tang, B.; Sun, D. MOFs-derived porous Mn2O3 as high-performance anode material for Li-ion battery. *J. Mater. Chem. A* **2015**, *3*, 5266−5269.

(5) Duan, J.; Chen, S.; Zhao, C. Ultrathin metal-organic framework array for efficient electrocatalytic water splitting. *Nat. Commun.* **2017**, *8*, No. 15341.

(6) Wang, W.; Xu, X.; Zhou, W.; Shao, Z. Recent Progress in Metal-Organic Frameworks for Applications in Electrocatalytic and Photocatalytic Water Splitting. *Adv. Sci.* **2017**, *4*, 1600371−1600392.

(7) Xiao, X.; Song, H.; Lin, S.; Zhou, Y.; Zhan, X.; Hu, Z.; Zhang, Q.; Sun, J.; Yang, B.; Li, T.; Jiao, L.; Zhou, J.; Tang, J.; Gogotsi, Y. Scalable salt-templated synthesis of two-dimensional transition metal oxides. *Nat. Commun.* **2016**, *7*, No. 11296.

(8) Wang, Q.; Xue, X.; Lei, Y.; Wang, Y.; Feng, Y.; Xiong, X.; Wang, D.; Li, Y. Engineering of Electronic States on Co3O4 Ultrathin Nanosheets by Cation Substitution and Anion Vacancies for Oxygen Evolution Reaction. *Small* **2020**, No. 2001571.

(9) Algara-Siller, G.; Severin, N.; Chong, S. Y.; Bjorkman, T.; Palgrave, R. G.; Laybourn, A.; Antonietti, M.; Khimyak, Y. Z.; Krasheninnikov, A. V.; Rabe, J. P.; Kaiser, U.; Cooper, A. I.; Thomas, A.; Bojdys, M. J. Triazine-based graphitic carbon nitride: a two-dimensional semiconductor. *Angew. Chem., Int. Ed.* **2014**, *53*, 7450−7455.

(10) Wang, Q.; Lei, Y.; Wang, Y.; Liu, Y.; Song, C.; Zeng, J.; Song, Y.; Duan, X.; Wang, D.; Li, Y. Atomic-scale engineering of chemical-vapor-deposition-grown 2D transition metal dichalcogenides for electrocatalysis *Energy Environ. Sci.* 2020. DOI: 10.1039/d0ee00450b.

(11) Liu, R.; Wang, Y.; Liu, D.; Zou, Y.; Wang, S. Water-Plasma-Enabled Exfoliation of Ultrathin Layered Double Hydroxide Nanosheets with Multivacancies for Water Oxidation. *Adv. Mater.* **2017**, *29*, 1701546−1701553.

(12) Zhou, Y.; Li, Z.; Liu, Y.; Huo, J.; Chen, C.; Li, Q.; Niu, S.; Wang, S. Regulating Hydrogenation Chemoselectivity of alpha,beta-Unsaturated Aldehydes by Combination of Transfer and Catalytic Hydrogenation. *ChemSusChem* **2020**, *13*, 1746−1750.

(13) Fang, G.; Wang, Q.; Zhou, J.; Lei, Y.; Chen, Z.; Wang, Z.; Pan, A.; Liang, S. Metal Organic Framework-Templated Synthesis of Bimetallic Selenides with Rich Phase Boundaries for Sodium-Ion Storage and Oxygen Evolution Reaction. *ACS Nano* **2019**, *13*, 5635−5645.

(14) Zhao, S.; Wang, Y.; Dong, J.; He, C.-T.; Yin, H.; An, P.; Zhao, K.; Zhang, X.; Gao, C.; Zhang, L.; Lv, J.; Wang, J.; Zhang, J.; Khattak, A. M.; Khan, N. A.; Wei, Z.; Zhang, J.; Liu, S.; Zhao, H.; Tang, Z. Ultrathin metal-organic framework nanosheets for electrocatalytic oxygen evolution. *Nat. Energy* **2016**, *1*, No. 16184.

(15) Xu, Y.; Li, B.; Zheng, S.; Wu, P.; Zhan, J.; Xue, H.; Xu, Q.; Pang, H. Ultrathin two-dimensional cobalt-organic framework nanosheets for high-performance electrocatalytic oxygen evolution. *J. Mater. Chem. A* **2018**, *6*, 22070−22076.

(16) Li, F. L.; Shao, Q.; Huang, X.; Lang, J. P. Nanoscale Trimetallic Metal-Organic Frameworks Enable Efficient Oxygen Evolution Electrocatalysis. *Angew. Chem., Int. Ed.* **2018**, *57*, 1888−1892.

(17) Li, F. L.; Wang, P.; Huang, X.; Young, D. J.; Wang, H. F.; Braunstein, P.; Lang, J. P. Large-Scale, Bottom-Up Synthesis of Binary Metal-Organic Framework Nanosheets for Efficient Water Oxidation. *Angew. Chem., Int. Ed.* **2019**, *58*, 7051−7056.

(18) Xu, H.; Fei, B.; Cai, G.; Ha, Y.; Liu, J.; Jia, H.; Zhang, J.; Liu, M.; Wu, R. Boronization-Induced Ultrathin 2D Nanosheets with Abundant Crystalline-Amorphous Phase Boundary Supported on Nickel Foam toward Efficient Water Splitting. *Adv. Energy Mater.* **2019**, *10*, No. 1902714.

(19) Tang, C.; Zhang, R.; Lu, W.; He, L.; Jiang, X.; Asiri, A. M.; Sun, X. Fe-Doped CoP Nanoarray: A Monolithic Multifunctional Catalyst for Highly Efficient Hydrogen Generation. *Adv. Mater.* **2017**, *29*, No. 1602441.

(20) Hao, S.; Chen, L.; Yu, C.; Yang, B.; Li, Z.; Hou, Y.; Lei, L.; Zhang, X. NiCoMo Hydroxide Nanosheet Arrays Synthesized via Chloride Corrosion for Overall Water Splitting. *ACS Energy Lett.* **2019**, *4*, 952−959.

(21) Chen, Z.; Fei, B.; Hou, M.; Yan, X.; Chen, M.; Qing, H.; Wu, R. Ultrathin Prussian blue analogue nanosheet arrays with open bimetal centers for efficient overall water splitting. *Nano Energy* **2020**, *68*, No. 104371.

(22) Mesbah, A.; Rabu, P.; Sibille, R.; Lebegue, S.; Mazet, T.; Malaman, B.; Francois, M. From hydrated Ni3(OH)2(C8H4O4)2(H2O)4 to anhydrous Ni2(OH)2(C8H4O4): impact of structural transformations on magnetic properties. *Inorg. Chem.* **2014**, *53*, 872−881.

(23) Hosono, E.; Fujihara, S.; Honma, I.; Ichihara, M.; Zhou, H. Synthesis of the CoOOH fine nanoflake film with the high rate capacitance property. *J. Power Sources* **2006**, *158*, 779−783.

(24) Yang, H.; Luo, S.; Bao, Y.; Luo, Y.; Jin, J.; Ma, J. In situ growth of ultrathin Ni-Fe LDH nanosheets for high performance oxygen evolution reaction. *Inorg. Chem. Front.* **2017**, *4*, 1173−1181.

(25) Elshahawy, A. M.; Ho, K. H.; Hu, Y.; Fan, Z.; Hsu, Y. W. B.; Guan, C.; Ke, Q.; Wang, J. Microwave-assisted hydrothermal synthesis of nanocrystal β-Ni(OH)2 for supercapacitor applications. *CrystEngComm* **2016**, *18*, 3256−3264.

(26) Chandramohan, P.; Srinivasan, M. P.; Velmurugan, S.; Narasimhan, S. V. Cation distribution and particle size effect on Raman spectrum of CoFe2O4. *J. Solid State Chem.* **2011**, *184*, 89−96.

(27) Mironova-Ulmane, N.; Kuzmin, A.; Steins, I.; Grabis, J.; Sildos, I.; Pärs, M. Raman scattering in nanosized nickel oxide NiO. *J. Phys.: Conf. Ser.* **2007**, *93*, No. 012039.

(28) Wang, B.; Shang, J.; Guo, C.; Zhang, J.; Zhu, F.; Han, A.; Liu, J. A General Method to Ultrathin Bimetal-MOF Nanosheets Arrays via In Situ Transformation of Layered Double Hydroxides Arrays. *Small* **2019**, *15*, 1804761−1804768.

(29) Zheng, Y.; Zheng, S.; Xu, Y.; Xue, H.; Liu, C.; Pang, H. Ultrathin two-dimensional cobalt-organic frameworks nanosheets for electrochemical energy storage. *Chem. Eng. J.* **2019**, *373*, 1319−1328.

(30) Zhu, D.; Guo, C.; Liu, J.; Wang, L.; Du, Y.; Qiao, S. Z. Two-dimensional metal-organic frameworks with high oxidation states for efficient electrocatalytic urea oxidation. *Chem. Commun.* **2017**, *53*, 10906−10909.

(31) Qian, Q.; Li, Y.; Liu, Y.; Yu, L.; Zhang, G. Ambient Fast Synthesis and Active Sites Deciphering of Hierarchical Foam-Like Trimetal-Organic Framework Nanostructures as a Platform for Highly Efficient Oxygen Evolution Electrocatalysis. *Adv. Mater.* **2019**, *31*, 1901139−1901147.

(32) Rui, K.; Zhao, G.; Chen, Y.; Lin, Y.; Zhou, Q.; Chen, J.; Zhu, J.; Sun, W.; Huang, W.; Dou, S. X. Hybrid 2D Dual-Metal-Organic Frameworks for Enhanced Water Oxidation Catalysis. *Adv. Funct. Mater.* **2018**, *28*, No. 1801554.

(33) Zhou, Q.; Chen, Y.; Zhao, G.; Lin, Y.; Yu, Z.; Xu, X.; Wang, X.; Liu, H. K.; Sun, W.; Dou, S. X. Active-Site-Enriched Iron-Doped Nickel/Cobalt Hydroxide Nanosheets for Enhanced Oxygen Evolution Reaction. *ACS Catal.* **2018**, *8*, 5382−5390.

(34) Yang, H.; Chen, Z.; Guo, P.; Fei, B.; Wu, R. B-doping-induced amorphization of LDH for large-current-density hydrogen evolution reaction. *Appl. Catal., B* **2020**, *261*, No. 118240.

(35) Yang, H.; Chen, Z.; Hao, W.; Xu, H.; Guo, Y.; Wu, R. Catalyzing overall water splitting at an ultralow cell voltage of 1.42 V via coupled Co-doped NiO nanosheets with carbon. *Appl. Catal., B* **2019**, *252*, 214−221.